Monthly Notices
of the
ROYAL ASTRONOMICAL SOCIETY

MNRAS **461,** 3964–3975 (2016)
Advance Access publication 2016 July 5

doi:10.1093/mnras/stw1596

Secular dynamics of gravitationally bound pair of binaries

David Vokrouhlický★

Instiute of Astronomy, Charles University, Prague, V Holešovičkách 2, CZ-180 00 Prague 8, Czech Republic

Accepted 2016 June 30. Received 2016 June 30; in original form 2016 May 16

ABSTRACT

Equations of secular dynamics for stellar quadruple systems in 2+2 hierarchy are formulated. Non-singular, angular momentum and Laplace vector variables are used to describe orbital evolution of both inner and outer orbits. Given a typical wide separation of the binaries in these systems, gravitational interactions are truncated at the octupole approximation. Secular equations are propagated numerically and the results compared to the complete numerical integration on a long time-scale. Our basic formulation uses a point-mass model, but we also extend it by including the simplest description of the quadrupole interaction among the components of close (inner) binaries. Evolution of orbital planes of the binaries is discussed analytically in a simplified model and numerically using a more complete model. Maximum angular separation of the two orbital planes reaches only 20–40 per cent of the simple geometric maximum value for low-eccentricity cases with small inclination with respect to the orbital plane of the relative motion. This may be a pre-requisite for occurrence of quadruple systems with both binaries showing eclipses. However, statistical occurrence of eclipses at any time for a synthetic population of quadruples with initially isotropic distribution of orbital planes is about equal to the model where the orbits do not evolve due to gravitational interactions. We also show that the model is potentially suitable for long-term studies of the initial evolutionary tracks of the 2 + 2 quadruple systems.

Key words: binaries: eclipsing – stars: kinematics and dynamics.

1 INTRODUCTION

Multiple stellar systems are observed at various long-term stable configurations. The case with four components comes in two variants, namely (i) a hierarchical 3+1 case (or (2+1)+1 case), a triple system accompanied by a fourth, distant component, and (ii) a 2+2 case, two binaries orbiting each other. Interestingly, the 2+2 configuration (ii) is found more common, representing about 4 per cent of multiple systems in total (Tokovinin 2008, 2014). It has been suggested that these systems form through a particular fragmentation sequence, different from that leading to the 3+1 case.

To unwind traces of the formation processes, if not fully masked by subsequent dynamical evolution, and/or to reveal statistical properties of components in multiple systems, it is important to well determine their physical parameters and geometrical architecture of their orbits. These parameters are better constrained when at least one of the binary component is eclipsing. The limited number of cases when both binaries in a 2+2 quadruple configuration are eclipsing are even more favourable to determine the system's geometry (e.g. Lee et al. 2008; Zasche & Uhlař 2013, 2016). Statistical chances of a system to be eclipsing at any time differ in single binaries and systems when the binary is a component in a multiple system (such as a triple or 2+2 quadruple). In the former case it is principally given by the expected initial isotropy of orbital planes in space. In the multiple system cases, the orientation of orbital planes of embedded binaries evolve in time and may favour or disfavour eclipses at occasions. The overall statistical expectations of the eclipsing phenomenon thus additionally require modelling of orbital interactions in the system.

Only few studies were devoted to the dynamics of quadruple systems in the 2+2 hierarchy so far (e.g. Pejcha et al. 2013). This is also because observational evidence of their orbital evolution is very limited (e.g. Pribulla et al. 2008). Most of the currently known systems are widely separated, implying evolution time-scales of thousands of years or longer (e.g. Tokovinin 2008). Some studies set general constraints on systems' evolution in non-generic geometries or a restricted parameter space (e.g. Roy & Steves 2000; Széll, Steves & Érdi 2004), but these are of a limited importance for general astronomical use. Beust (2003) presented fast and efficient numerical scheme of propagation of stellar orbits in multiple stellar systems (including our 2+2 hierarchy). While powerful as a tool, it still requires an integration timestep of a fraction of the shortest orbital period of a participating subsystem. To grasp some characteristics of the system's long-term evolution, it might be therefore interesting to have a faster, though possibly less precise, framework.

★ E-mail: vokrouhl@cesnet.cz

This is provided by the secular approach (e.g. Morbidelli 2002), in which details of the orbital evolution on a time-scale shorter than that of inner and outer binaries is neglected and the system evolution is studied on longer time-scales. Recently, Hamers & Portegies Zwart (2016) presented a general scheme of the first-order secular theory applicable to nested multiple systems.[1] Their approach obviously includes also quadruples in the 2 + 2 architecture. While very interesting, we find our paper adds discussion of new topics, such as coplanarity of the binary subsystems. Moreover, being tailored to the 2 + 2 architecture from scratch, it is little easier to discern results in our case than in the very general set-up of Hamers & Portegies Zwart (2016).

In this paper, we introduce the simplest equations for the secular dynamics of the 2+2 orbital hierarchy of quadruple stellar systems (Section 2). We use them to analyse coupling of the orbital planes of the close binaries in the 2+2 systems. We find this happens to be higher than expected from simple geometrical arguments for systems that are near coplanar. This result may imply higher chances for eclipses in both binaries. However, assuming a larger sample of 2+2 systems with initially isotropic distribution of orbital planes the advantages disappears. In Section 3.3, we show that the statistical occurrence of eclipses at any moment of time is on average the same as for dynamically non-evolving (static) systems. In Section 4, we demonstrate applicability of our approach for studies of interaction of the binary systems in the Kozai–Lidov (KL) regime that may result in colourful evolutionary tracks. Conclusions, with a brief discussion of two interesting quadruple systems, are summarized in Section 5.

2 THEORY

To set the stage, we start by introducing a simplified model in which all stars in the system are point masses. Interestingly, the orbital evolution is well approximated by a couple of interacting triple-star systems. One can thus readily develop a reasonable secular approximation of the system's motion and even, in certain conditions, obtain a constraint on tilt between the orbital planes of the eclipsing binaries. Stellar proximity in the close binaries requires in general to include additional dynamical effects, namely (i) quadrupole and higher order terms due to interaction of stars modelled as extended bodies, (ii) tidal interaction, and (iii) spin-orbit coupling. Some of these effects are considered in this paper. However, we do so only to the level needed to explain the observations since a more complete work would inevitably involve large number of free parameters. At this moment it is not our intention to fully analyse their impact on the results.

2.1 Notation

Denote A and B the two close binaries which together constitute the quadruple system A-B. Masses of components in A are $m_{\rm Aa}$ and $m_{\rm Ab}$, similarly masses in B are $m_{\rm Ba}$ and $m_{\rm Bb}$. It is also useful to introduce $M_{\rm A} = m_{\rm Aa} + m_{\rm Ab}$, the total mass in A, $m'_{\rm A} = m_{\rm Aa}m_{\rm Ab}/M_{\rm A}$, the reduced mass in A, and $X_{\rm Aa} = m_{\rm Aa}/M_{\rm A}$ and $X_{\rm Ab} = m_{\rm Ab}/M_{\rm A}$, which denote the mass fraction of the two stellar components in the subsystem A. The corresponding quantities in B are $M_{\rm B} = m_{\rm Ba} + m_{\rm Bb}$, $m'_{\rm B} = m_{\rm Ba}m_{\rm Bb}/M_{\rm B}$, and $X_{\rm Ba} = m_{\rm Ba}/M_{\rm B}$ and $X_{\rm Bb} = m_{\rm Bb}/M_{\rm B}$. Finally, $M_{\rm AB} = M_{\rm A} + M_{\rm B}$ is the total mass of the system and $m'_{\rm AB} = M_{\rm A}M_{\rm B}/M_{\rm AB}$ the reduced mass associated with the relative motion of A and B about the centre-of-mass of the system. The nature of the system, (2,2) hierarchy (see, Milani & Nobili 1983), dictates a preferred coordinate system: (i) $\boldsymbol{r}_{\rm A}$ is the relative position of Ab with respect to Aa, (ii) $\boldsymbol{r}_{\rm B}$ is the relative position of Bb with respect to Ba, and (iii) $\boldsymbol{R}$ is the relative position of the centre-of-mass of B with respect to the centre-of-mass of A.[2] The corresponding conjugate momenta are $\boldsymbol{p}_{\rm A}$, $\boldsymbol{p}_{\rm B}$ and $\boldsymbol{P}$. Obviously, a one-to-one transformation between the four star positions in an arbitrary inertial system and our variables requires to complement them by position $\boldsymbol{T}$ of the overall centre-of-mass of the system (and the related momentum). Assuming the system is isolated, the last degrees of freedom are ignorable, because they result only in linear motion of $\boldsymbol{T}$, and observationally, would result in a simple systemic velocity of the whole quadruple system. For that reason we do not need to consider $\boldsymbol{T}$ in our analysis.

Dynamics of the quadruple system in a reduced phase space $(\boldsymbol{r}_{\rm A}, \boldsymbol{r}_{\rm B}, \boldsymbol{R}; \boldsymbol{p}_{\rm A}, \boldsymbol{p}_{\rm B}, \boldsymbol{P})$ follows from the Hamiltonian

$$\mathcal{H} = \mathcal{H}_{\rm A}\left(\boldsymbol{r}_{\rm A}, \boldsymbol{p}_{\rm A}\right) + \mathcal{H}_{\rm B}\left(\boldsymbol{r}_{\rm B}, \boldsymbol{p}_{\rm B}\right) + \mathcal{H}_{\rm AB}\left(\boldsymbol{R}, \boldsymbol{P}\right) + \mathcal{H}_{\rm int}\left(\boldsymbol{r}_{\rm A}, \boldsymbol{r}_{\rm B}, \boldsymbol{R}\right) + \mathcal{H}'_{\rm int}\left(\boldsymbol{r}_{\rm A}, \boldsymbol{r}_{\rm B}, \boldsymbol{R}\right), \quad (1)$$

where the first row highlights separation on to three integrable, uncoupled two-body motions

$$\mathcal{H}_{\rm A}\left(\boldsymbol{r}_{\rm A}, \boldsymbol{p}_{\rm A}\right) = \frac{\boldsymbol{p}_{\rm A}^2}{2\,m'_{\rm A}} - G\,\frac{m'_{\rm A}M_{\rm A}}{r_{\rm A}}, \quad (2)$$

$$\mathcal{H}_{\rm B}\left(\boldsymbol{r}_{\rm B}, \boldsymbol{p}_{\rm B}\right) = \frac{\boldsymbol{p}_{\rm B}^2}{2\,m'_{\rm B}} - G\,\frac{m'_{\rm B}M_{\rm B}}{r_{\rm B}}, \quad (3)$$

$$\mathcal{H}_{\rm AB}\left(\boldsymbol{R}, \boldsymbol{P}\right) = \frac{\boldsymbol{P}^2}{2\,m'_{\rm AB}} - G\,\frac{m'_{\rm AB}M_{\rm AB}}{R}. \quad (4)$$

The second-row terms $\mathcal{H}_{\rm int}$ and $\mathcal{H}'_{\rm int}$ express a plethora of mutual interactions. Interestingly, there is a particular hierarchy in the interaction terms which justifies to organize them in the two mentioned terms.

The leading-order interaction term is given by the $\mathcal{H}_{\rm int}$ which reads:

$$\mathcal{H}_{\rm int} = -G\,\frac{m'_{\rm AB}M_{\rm AB}}{R}\sum_{n\geq 2}\chi_{{\rm A},n}\left(\frac{r_{\rm A}}{R}\right)^n P_n\left(\gamma_{\rm A}\right) - G\,\frac{m'_{\rm AB}M_{\rm AB}}{R}\sum_{n\geq 2}\chi_{{\rm B},n}\left(\frac{r_{\rm B}}{R}\right)^n P_n\left(\gamma_{\rm B}\right), \quad (5)$$

where we introduced non-dimensional coefficients[3]

$$\chi_{{\rm A},n} = X_{\rm Aa}X_{\rm Ab}\left[X_{\rm Aa}^{n-1} - (-X_{\rm Ab})^{n-1}\right], \quad (6)$$

$$\chi_{{\rm B},n} = X_{\rm Ba}X_{\rm Bb}\left[X_{\rm Bb}^{n-1} - (-X_{\rm Ba})^{n-1}\right]. \quad (7)$$

Note that equal-mass binaries have $\chi_n = 0$ for odd-degree multipoles n and, as expected, the series in (5) start with a quadrupole

[1] We were not aware of this work prior submission of this paper.

[2] See also Beust (2003) in whose notation our variables are called hierarchical Jacobi coordinates.

[3] Note the reverse order of 'a' and 'b' components in the definition of the χ-coefficients. Alternately, see Milani & Nobili (1983), one could define $\chi_{{\rm B},n} = X_{\rm Ba}X_{\rm Bb}\left[X_{\rm Ba}^{n-1} - (-X_{\rm Bb})^{n-1}\right]$ and use $P_n(-\gamma_{\rm B})$ in the right-hand side of equation (5).

contribution ($n = 2$). The arguments in Legendre polynomials P_n are expectedly cosines of mutual angles of the $\boldsymbol{r}_{\rm A}$-$\boldsymbol{R}$ and $\boldsymbol{r}_{\rm B}$-$\boldsymbol{R}$ pairs:

$$\gamma_{\rm A} = \frac{\boldsymbol{R}\cdot\boldsymbol{r}_{\rm A}}{R\,r_{\rm A}}, \tag{8}$$

$$\gamma_{\rm B} = \frac{\boldsymbol{R}\cdot\boldsymbol{r}_{\rm B}}{R\,r_{\rm B}}. \tag{9}$$

Note there is no direct $\boldsymbol{r}_{\rm A}$-$\boldsymbol{r}_{\rm B}$ interaction in (5) and the overall structure can be interpreted as coupled evolution of two triple systems: (i) pair A interacting with body of total mass $M_{\rm B}$ located in the centre-of-mass of the system B, and (ii) pair B interacting with body of total mass $M_{\rm A}$ located in the centre-of-mass of the system A. Assuming $r_{\rm A} \simeq r_{\rm B}$, interaction Hamiltonian (5) is of the second order in a small parameter $\varepsilon \simeq r_{\rm A}/R \simeq r_{\rm B}/R$ if compared to the Hamiltonian terms (2)–(4). In what follows, we shall primarily restrict to the quadrupole truncation in (5). This is because in our exemplary case of V994 Her (i) the small parameter $\varepsilon \simeq 1/80$, and (ii) additionally both pairs A and B have stellar components of comparable masses (suppressing thus the role of the octupole term).

The second interaction term $\mathcal{H}'_{\rm int}$ in (1) has a more complicated structure and exhibits all possible couplings of the $\boldsymbol{r}_{\rm A}$, $\boldsymbol{r}_{\rm B}$ and $\boldsymbol{R}$ vectors. Fortunately, $\mathcal{H}'_{\rm int} \sim \varepsilon^4$ (e.g. Milani & Nobili 1983, and equation 10 below) and thus it is less important than the quadrupole and octupole terms in (5). For sake of completeness we give the principal part (omitting the order ε^5 and higher)

$$\mathcal{H}'_{\rm int} = -\frac{3\,Gm'_{\rm A}m'_{\rm B}}{4\,R}\left(\frac{r_{\rm A}r_{\rm B}}{R^2}\right)^2\Big(11 - 15\,\gamma_{\rm A}^2 - 15\,\gamma_{\rm B}^2 - 8\,\gamma_{\rm AB}^2 + 35\,\gamma_{\rm A}^2\,\gamma_{\rm B}^2\Big), \tag{10}$$

with

$$\gamma_{\rm AB} = \frac{\boldsymbol{r}_{\rm A}\cdot\boldsymbol{r}_{\rm B}}{r_{\rm A}\,r_{\rm B}}. \tag{11}$$

$\mathcal{H}'_{\rm int}$, together with the higher multipole terms in (5), would be required for tracking longer term orbital evolution of the system, but at this moment we shall not need them.

In passing we mention that at least two quadruple systems in the 2 + 2 hierarchy were suggested to reside in mutual $P_{\rm B}/P_{\rm A} \simeq 3/2$ mean motion resonance (e.g. Ofir 2008; Cagaš & Pejcha 2012; Kołaczkowski et al. 2013). These situation, however, present an interesting and intrigue problem, because the relevant dynamical coupling (10) is rather weak, as mentioned above. Long-term stability of the suggested resonant configuration is speculative and has not been studied yet.

2.2 First-order secular approach

Moving now towards the perturbation approach, the secular theory in particular, we transform the conjugated coordinates and momenta to orbital elements. From the plethora of possible choices we adopt the following set (e.g. Breiter & Ratajczak 2005, and references therein): (i) semimajor axis a, (ii) normalized (non-dimensional) angular momentum vector $\boldsymbol{K} = \sqrt{1-e^2}\,\boldsymbol{k}$, where e is the orbital eccentricity and $\boldsymbol{k}$ unit vector normal to the orbital plane, (iii) normalized (non-dimensional) Laplace vector $\pi = e\,\boldsymbol{p}$, where $\boldsymbol{p}$ is the unit vector directed to the pericentre, and (iv) longitude in orbit λ. The apparent overparametrization is due to existence of two constraints: $\boldsymbol{K}\cdot\pi = 0$ and $\boldsymbol{K}^2 + \pi^2 = 1$. Conveniently, the adopted orbital elements (a, $\boldsymbol{K}$, π, λ) are non-singular, allowing thus to analyse all possible orbital configurations including small values of eccentricity and inclination. Additionally, when λ is eliminated from the mean Hamiltonian, as in the secular theory, the resulting perturbation equations have readily a form valid in an arbitrary reference system. As in the case of coordinates and momenta, the orbital elements of the binaries A and B are denoted ($a_{\rm A}$, $\boldsymbol{K}_{\rm A}$, $\pi_{\rm A}$, $\lambda_{\rm A}$) and ($a_{\rm B}$, $\boldsymbol{K}_{\rm B}$, $\pi_{\rm B}$, $\lambda_{\rm B}$), and the orbital elements of the relative motion of centre-of-mass B with respect to the centre-of-mass A are simply (a, $\boldsymbol{K}$, π, λ).

With these elements at hand, the two-body parts (2)–(4) of the Hamiltonian transform to their simple Keplerian values: (i) $\mathcal{H}_{\rm A}(a_{\rm A}) = -G\,m'_{\rm A}M_{\rm A}/(2a_{\rm A})$, (ii) $\mathcal{H}_{\rm B}(a_{\rm B}) = -G\,m'_{\rm B}M_{\rm B}/(2a_{\rm B})$, and (iii) $\mathcal{H}_{\rm AB}(a) = -G\,m'_{\rm AB}M_{\rm AB}/(2a)$. These allow us to define unperturbed mean motion values $n_{\rm A}$, $n_{\rm B}$ and n using (i) $n_{\rm A}^2 a_{\rm A}^3 = GM_{\rm A}$, (ii) $n_{\rm B}^2 a_{\rm B}^3 = GM_{\rm B}$, and (iii) $n^2a^3 = GM_{\rm AB}$. The corresponding unperturbed orbital periods are $P_{\rm A}$, $P_{\rm B}$, and P.

It is notoriously quite more difficult to express the interaction potential energy ($\mathcal{H}_{\rm int} + \mathcal{H}'_{\rm int}$) in terms of the orbital elements of all three orbital components (see e.g. Appendices in Hamers & Portegies Zwart 2016). Typically, one would obtain its form in (i) power-series of semimajor axes and scalar products of $\boldsymbol{K}$ and π variables, and (ii) Fourier series in longitudes in orbit. Luckily, we shall not need such a complete form of the perturbing potential because our goal is to provide characterization of the long-term orbital evolution using secular approach. We assume short-period variations have sufficiently small amplitude, which is always true unless mean motion resonances are present (see above).

In the secular approach one seeks a coordinate transformation which allows us to eliminate fast variables $\lambda_{\rm A}$, $\lambda_{\rm B}$, and λ from the perturbing potential energy ($\mathcal{H}_{\rm int} + \mathcal{H}'_{\rm int}$), thereby defining the mean perturbation potential energy $\overline{\mathcal{H}} = \overline{\mathcal{H}}_{\rm int} + \overline{\mathcal{H}}'_{\rm int}$. While a systematic fast-variable elimination to any order in small parameter ε may be cumbersome procedure (e.g. Morbidelli 2002), we shall restrict to the lowest order theory. In this case, we use the quadrupole and octupole parts in $\mathcal{H}_{\rm int}$ and the corresponding $\overline{\mathcal{H}}_{\rm int}$ is a mere orbital average of $\mathcal{H}_{\rm int}$ over unperturbed cycles of A, B, and A-B revolution.[4] In order to specify which part we have in mind, we shall denote $\overline{\mathcal{H}}_2$ the average of the quadrupole part in $\mathcal{H}_{\rm int}$ and $\overline{\mathcal{H}}_3$ the average of the octupole part in $\mathcal{H}_{\rm int}$. So altogether $\overline{\mathcal{H}} = \overline{\mathcal{H}}_2 + \overline{\mathcal{H}}_3$ in our case.

The immediate consequence of the fast-variable elimination in $\overline{\mathcal{H}}$ is that the semimajor axes $a_{\rm A}$, $a_{\rm B}$, and a are integrals of motion and remain constant. The mean values of $\boldsymbol{K}$ and π for each of the orbital components remain the only active variables. The corresponding dynamical equations for binaries A and B read (e.g. Breiter & Ratajczak 2005; Tremaine, Touma & Namouni 2009; Farago & Laskar 2010; Rosengren & Scheeres 2014; Liu, Muñoz & Lai 2015)

$$\frac{{\rm d}\boldsymbol{K}_{\rm A}}{{\rm d}t} = -\frac{1}{\Lambda_{\rm A}}\left(\pi_{\rm A}\times\frac{\partial\overline{\mathcal{H}}}{\partial\pi_{\rm A}} + \boldsymbol{K}_{\rm A}\times\frac{\partial\overline{\mathcal{H}}}{\partial\boldsymbol{K}_{\rm A}}\right), \tag{12}$$

$$\frac{{\rm d}\pi_{\rm A}}{{\rm d}t} = -\frac{1}{\Lambda_{\rm A}}\left(\boldsymbol{K}_{\rm A}\times\frac{\partial\overline{\mathcal{H}}}{\partial\pi_{\rm A}} + \pi_{\rm A}\times\frac{\partial\overline{\mathcal{H}}}{\partial\boldsymbol{K}_{\rm A}}\right), \tag{13}$$

$$\frac{{\rm d}\boldsymbol{K}_{\rm B}}{{\rm d}t} = -\frac{1}{\Lambda_{\rm B}}\left(\pi_{\rm B}\times\frac{\partial\overline{\mathcal{H}}}{\partial\pi_{\rm B}} + \boldsymbol{K}_{\rm B}\times\frac{\partial\overline{\mathcal{H}}}{\partial\boldsymbol{K}_{\rm B}}\right), \tag{14}$$

[4] Second-order quadrupole contributions would be necessary to include consistently $n = 4$ in $\mathcal{H}_{\rm int}$ and also $\mathcal{H}'_{\rm int}$ (see e.g. Breiter & Vokrouhlický 2015, for clarification).

$$\frac{\mathrm{d}\pi_\mathrm{B}}{\mathrm{d}t} = -\frac{1}{\Lambda_\mathrm{B}}\left(\boldsymbol{K}_\mathrm{B}\times\frac{\partial\overline{\mathcal{H}}}{\partial\pi_\mathrm{B}}+\pi_\mathrm{B}\times\frac{\partial\overline{\mathcal{H}}}{\partial\boldsymbol{K}_\mathrm{B}}\right), \tag{15}$$

where we denoted $\Lambda_\mathrm{A} = m'_\mathrm{A}\,n_\mathrm{A}a_\mathrm{A}^2$ and $\Lambda_\mathrm{B} = m'_\mathrm{B}\,n_\mathrm{B}a_\mathrm{B}^2$. Similarly,

$$\frac{\mathrm{d}\boldsymbol{K}}{\mathrm{d}t} = -\frac{1}{\Lambda}\left(\pi\times\frac{\partial\overline{\mathcal{H}}}{\partial\pi}+\boldsymbol{K}\times\frac{\partial\overline{\mathcal{H}}}{\partial\boldsymbol{K}}\right), \tag{16}$$

$$\frac{\mathrm{d}\pi}{\mathrm{d}t} = -\frac{1}{\Lambda}\left(\boldsymbol{K}\times\frac{\partial\overline{\mathcal{H}}}{\partial\pi}+\pi\times\frac{\partial\overline{\mathcal{H}}}{\partial\boldsymbol{K}}\right), \tag{17}$$

with $\Lambda = m'_\mathrm{AB}\,na^2$, holds for the elements of the relative orbit A-B. Once $\overline{\mathcal{H}}$ is determined, the secular system (12)–(17) is to be integrated numerically. This is because in generic cases there are no additional first integrals apart from: (i) conservation of the total angular momentum $\Lambda_\mathrm{A}\,\boldsymbol{K}_\mathrm{A}+\Lambda_\mathrm{B}\,\boldsymbol{K}_\mathrm{B}+\Lambda\,\boldsymbol{K}$, and (ii) conservation of energy $\overline{\mathcal{H}}$. The major advantage though is that the mean orbital elements $(\boldsymbol{K}_\mathrm{A},\pi_\mathrm{A};\boldsymbol{K}_\mathrm{B},\pi_\mathrm{B};\boldsymbol{K},\pi)$ change only very little on the orbital time-scales. Thus a much longer integration timestep, typically years, can used to propagate the secular system (12)–(17).

Because the quadrupole and octupole parts in $\mathcal{H}_\mathrm{int}$ are equivalent to a pair of interacting triple systems, it is straightforward to borrow results from triple-star dynamics studies to obtain the corresponding mean value $\overline{\mathcal{H}}$ of the Hamiltonian.

2.2.1 *Quadrupole interaction*

The quadrupole level has been extensively studied in both planetary and stellar context. The mean Hamiltonian part may be widely found, and is provided by Farago & Laskar (2010), Liu et al. (2015) or Breiter & Vokrouhlický (2015) in the vectorial elements adopted in this paper. We have

$$\begin{aligned}\overline{\mathcal{H}}_2 = &-\frac{C_\mathrm{A}}{\eta^5}\left[\eta^2\left(6e_\mathrm{A}^2-1\right)+3\left(\boldsymbol{K}_\mathrm{A}\cdot\boldsymbol{K}\right)^2-15\left(\pi_\mathrm{A}\cdot\boldsymbol{K}\right)^2\right]\\ &-\frac{C_\mathrm{B}}{\eta^5}\left[\eta^2\left(6e_\mathrm{B}^2-1\right)+3\left(\boldsymbol{K}_\mathrm{B}\cdot\boldsymbol{K}\right)^2-15\left(\pi_\mathrm{B}\cdot\boldsymbol{K}\right)^2\right],\end{aligned} \tag{18}$$

where $\eta = \sqrt{1-e^2}$ and

$$C_\mathrm{A} = \frac{1}{8}\,G\,\frac{m'_\mathrm{A}M_\mathrm{B}}{a}\left(\frac{a_\mathrm{A}}{a}\right)^2, \tag{19}$$

$$C_\mathrm{B} = \frac{1}{8}\,G\,\frac{M_\mathrm{A}m'_\mathrm{B}}{a}\left(\frac{a_\mathrm{B}}{a}\right)^2. \tag{20}$$

Obviously, $e_\mathrm{A}^2 = \pi_\mathrm{A}\cdot\pi_\mathrm{A}$, $e_\mathrm{B}^2 = \pi_\mathrm{B}\cdot\pi_\mathrm{B}$, and $e^2 = \pi\cdot\pi$. The system of secular equations (12)–(17) with $\overline{\mathcal{H}}_2$ included is fairly complex and does not admit general analytic solution. There is only one straightforward additional integral of motion, namely the eccentricity e of the relative orbit of the two binary systems at this level, a consequence of the fact that $\overline{\mathcal{H}}_2$ depends on π only through $e^2 = \pi\cdot\pi$. On the contrary, both e_A and e_B are generally not conserved except for admitted $e_\mathrm{A} = 0$ and $e_\mathrm{B} = 0$ solutions. It is well known (e.g. Farago & Laskar 2010) that the zero eccentricity solutions are stable only when the mutual inclination of the orbital plane of the corresponding binary A or B and the orbital plane of the relative motion A-B is less than a certain limit (roughly 40°). If the mutual inclination of these orbital planes is larger, the zero eccentricity solution of the binary is unstable and it is necessarily pushed to have large oscillations (unless tidal effect keeps again the eccentricity smaller than some limit). This is the Kozai regime (e.g. Söderhjelm 1982; Morbidelli 2002; Khodykin, Zakharov & Andersen 2004; Fabrycky & Tremaine 2007).

2.2.2 *Octupole interaction*

Systems with unequal mass components in eclipsing pairs, and those with large enough ε parameter, may require to include the octupole term in $\overline{\mathcal{H}}$. This is done through (e.g. Breiter & Vokrouhlický 2015; Liu et al. 2015)

$$\begin{aligned}\overline{\mathcal{H}}_3 = &-\frac{C'_\mathrm{A}}{\eta^7}\left[\left(\pi_\mathrm{A}\cdot\pi\right)\,G_\mathrm{A}-10\left(\pi_\mathrm{A}\cdot\boldsymbol{K}\right)\left(\pi\cdot\boldsymbol{K}_\mathrm{A}\right)\left(\boldsymbol{K}_\mathrm{A}\cdot\boldsymbol{K}\right)\right]\\ &-\frac{C'_\mathrm{B}}{\eta^7}\left[\left(\pi_\mathrm{B}\cdot\pi\right)\,G_\mathrm{B}-10\left(\pi_\mathrm{B}\cdot\boldsymbol{K}\right)\left(\pi\cdot\boldsymbol{K}_\mathrm{B}\right)\left(\boldsymbol{K}_\mathrm{B}\cdot\boldsymbol{K}\right)\right],\end{aligned} \tag{21}$$

where we abbreviated

$$G_\mathrm{A} = \left(1-8e_\mathrm{A}^2\right)\eta^2-5\left(\boldsymbol{K}_\mathrm{A}\cdot\boldsymbol{K}\right)^2+35\left(\pi_\mathrm{A}\cdot\boldsymbol{K}\right)^2, \tag{22}$$

$$G_\mathrm{B} = \left(1-8e_\mathrm{B}^2\right)\eta^2-5\left(\boldsymbol{K}_\mathrm{B}\cdot\boldsymbol{K}\right)^2+35\left(\pi_\mathrm{B}\cdot\boldsymbol{K}\right)^2, \tag{23}$$

and the constant factors read

$$C'_\mathrm{A} = \frac{15}{64}\,G\,\frac{m'_\mathrm{A}M_\mathrm{B}}{a}\left(X_\mathrm{Aa}-X_\mathrm{Ab}\right)\left(\frac{a_\mathrm{A}}{a}\right)^3, \tag{24}$$

$$C'_\mathrm{B} = \frac{15}{64}\,G\,\frac{M_\mathrm{A}m'_\mathrm{B}}{a}\left(X_\mathrm{Bb}-X_\mathrm{Ba}\right)\left(\frac{a_\mathrm{B}}{a}\right)^3. \tag{25}$$

Now e is not any more constant, but often its variations are limited thanks to smallness of the octupole perturbation.

2.3 Approximate analytical constraint on mutual inclination of the A and B orbital planes

While the equations of the secular system must be integrated numerically in general, a useful approximation could be obtained by assuming zero, or small, eccentricities of the binaries A and B and restricting to the quadrupole interaction $\overline{\mathcal{H}} = \overline{\mathcal{H}}_2$. Sufficiently small inclination of both A and B orbital planes to the orbital plane of the A-B motion, or strong tidal interaction in A and B, guarantees consistency of such assumption.

Setting thus $e_\mathrm{A} = e_\mathrm{B} = 0$, with e arbitrary constant, we now have the fundamental set of variables reduced to unit vectors $\boldsymbol{k}_\mathrm{A}$, $\boldsymbol{k}_\mathrm{B}$, and $\boldsymbol{k}$ normal to the respective orbital planes. One easily checks their evolution satisfies

$$\frac{\mathrm{d}\boldsymbol{k}_\mathrm{A}}{\mathrm{d}t} = \sigma_1\,\left(\boldsymbol{k}_\mathrm{A}\cdot\boldsymbol{k}\right)\left(\boldsymbol{k}_\mathrm{A}\times\boldsymbol{k}\right), \tag{26}$$

$$\frac{\mathrm{d}\boldsymbol{k}_\mathrm{B}}{\mathrm{d}t} = \sigma_2\,\left(\boldsymbol{k}_\mathrm{B}\cdot\boldsymbol{k}\right)\left(\boldsymbol{k}_\mathrm{B}\times\boldsymbol{k}\right), \tag{27}$$

$$\frac{\mathrm{d}\boldsymbol{k}}{\mathrm{d}t} = \sigma\,\left(\boldsymbol{k}\cdot\boldsymbol{k}_\mathrm{A}\right)\left(\boldsymbol{k}\times\boldsymbol{k}_\mathrm{A}\right)+\sigma'\,\left(\boldsymbol{k}\cdot\boldsymbol{k}_\mathrm{B}\right)\left(\boldsymbol{k}\times\boldsymbol{k}_\mathrm{B}\right), \tag{28}$$

with the corresponding fundamental frequencies

$$\sigma_1 = -\frac{3}{4\eta^3}\,n\,\frac{n}{n_\mathrm{A}}\,\frac{M_\mathrm{B}}{M_\mathrm{AB}}, \tag{29}$$

$$\sigma_2 = -\frac{3}{4\eta^3}\,n\,\frac{n}{n_\mathrm{B}}\,\frac{M_\mathrm{A}}{M_\mathrm{AB}}, \tag{30}$$

$$\sigma = -\frac{3}{4\eta^4}\, n\, X_{\rm Aa} X_{\rm Ab} \left(\frac{a_{\rm A}}{a}\right)^2, \tag{31}$$

$$\sigma' = -\frac{3}{4\eta^4}\, n\, X_{\rm Ba} X_{\rm Bb} \left(\frac{a_{\rm B}}{a}\right)^2. \tag{32}$$

Equations (26)–(28) describe precession motion of the normal vectors about each other. Unfortunately, they still have too many degrees of freedom to possess an easy analytic solution. Nevertheless, they admit useful first integrals[5]

$$C_1 = \sigma\, x^2 + \sigma'\, y^2, \tag{33}$$

$$C_2 = \frac{\sigma_2}{\sigma'}\, x + \frac{\sigma_1}{\sigma}\, y + z, \tag{34}$$

where we introduced $x = \boldsymbol{k}_{\rm A}\cdot\boldsymbol{k}$, $y = \boldsymbol{k}_{\rm B}\cdot\boldsymbol{k}$, and $z = \boldsymbol{k}_{\rm A}\cdot\boldsymbol{k}_{\rm B}$. Equations (33) and (34) indicate that the motion in the (x, y, z) space is constraint to the intersection of an elliptic cylinder and a plane. Given some initial values (x_0, y_0, z_0) for these parameters, it is easy to determine minimum value $z_{\rm min}$ of the z coordinate on that intersection, namely

$$z_{\rm min} = z_0 + \frac{\sigma_2}{\sigma'}\, x_0 + \frac{\sigma_1}{\sigma}\, y_0 - \sqrt{\left(\frac{x_0^2}{\sigma'} + \frac{y_0^2}{\sigma}\right)\left(\frac{\sigma_1^2}{\sigma} + \frac{\sigma_2^2}{\sigma'}\right)}. \tag{35}$$

The previous analysis of (26)–(28) does not take into account the obvious constraints $|x| \le 1$, $|y| \le 1$ and $|z| \le 1$, which formally represent a 'unitary' cube in the (x, y, z). Intersecting the $|x| \le 1$ and $|y| \le 1$ prism with the plane (34) we obtain an alternative constraint on the minimum value of the z coordinate, namely

$$z_{\rm min} = z_0 + \frac{\sigma_2}{\sigma'}\,(x_0 - 1) + \frac{\sigma_1}{\sigma}\,(y_0 - 1)\,. \tag{36}$$

In some cases (36) may be stronger constraint than (35), thus the resulting $z_{\rm min}$ is minimum of either value.

Denoting the mutual angle of the A and B system orbital planes by $\mathcal{J}_{\rm AB}$, we can use $z_{\rm min}$ from (35) and (36) to set an estimate of its maximum value $\mathcal{J}_{\rm AB}^{\rm max}$. Notably, when $|z_{\rm min}| \le 1$, we have $\cos\mathcal{J}_{\rm AB}^{\rm max} = z_{\rm min}$.

In order to demonstrate usefulness of the previous constraint, we conducted the following experiment. Denote $\mathcal{J}_{\rm A}$ and $\mathcal{J}_{\rm B}$ the angle between vectors $\boldsymbol{k}_{\rm A}$ and $\boldsymbol{k}$ ($\cos\mathcal{J}_{\rm A} = \boldsymbol{k}_{\rm A}\cdot\boldsymbol{k} = x$) and $\boldsymbol{k}_{\rm B}$ and $\boldsymbol{k}$ ($\cos\mathcal{J}_{\rm B} = \boldsymbol{k}_{\rm B}\cdot\boldsymbol{k} = y$). In the most simple approach one would approximate $\boldsymbol{k}$ fixed in the inertial space, by virtue of holding dominant part of the total angular momentum of the system, and assume only evolution of $\boldsymbol{k}_{\rm A}$ and $\boldsymbol{k}_{\rm B}$. These would exhibit steady precession about $\boldsymbol{k}$ with frequencies $\sigma_1\cos\mathcal{J}_{\rm A}$ and $\sigma_2\cos\mathcal{J}_{\rm B}$ as readily described by equations (26) and (27). Given enough time, the mutual angle $\mathcal{J}_{\rm AB}$ of the orbital planes of binary systems A and B would range from a minimum value $|\mathcal{J}_{\rm A} - \mathcal{J}_{\rm B}|$ to a maximum value $(\mathcal{J}_{\rm A} + \mathcal{J}_{\rm B})$ (note the $\mathcal{J}_{\rm A}$ and $\mathcal{J}_{\rm B}$ are preserved in this model). The latter would thus be the 'naively' estimated maximum value of $\mathcal{J}_{\rm AB}$. The reality is more complicated though, because the vector $\boldsymbol{k}$ itself evolves as described by equation (28). Henceforth, the maximum $\mathcal{J}_{\rm AB}^{\rm max}$ value is given rather by $z_{\rm min}$ described above and, as a rule of thumb, is smaller than or equal to $(\mathcal{J}_{\rm A} + \mathcal{J}_{\rm B})$. To see this effect, we evaluated function $F = 1 - \mathcal{J}_{\rm AB}^{\rm max}/(\mathcal{J}_{\rm A} + \mathcal{J}_{\rm B})$ for values $\mathcal{J}_{\rm A}$ and $\mathcal{J}_{\rm B}$ smaller than 30° in order to meet the condition of zero eccentricities of the A and B binaries. The value $F = 0$ implies that the sum $(\mathcal{J}_{\rm A} + \mathcal{J}_{\rm B})$ sets the maximum $\mathcal{J}_{\rm AB}$ value, but when $F > 0$, $\mathcal{J}_{\rm AB}^{\rm max} < \mathcal{J}_{\rm A} + \mathcal{J}_{\rm B}$, and $\mathcal{J}_{\rm AB}^{\rm max}$ strengthens the limit by which the orbital planes of A and B systems would maximally differ.

[5] These integrals may be also obtained from the general integrals of energy and total angular momentum of the quadruple system.

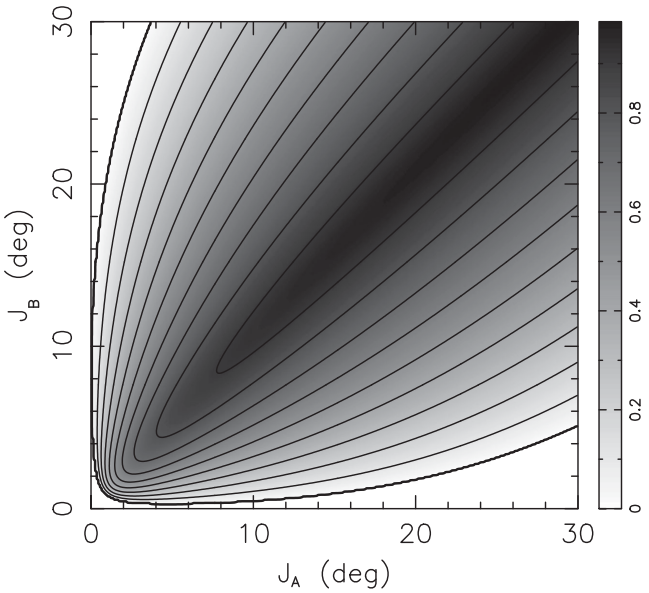

Figure 1. Isolevels of the F-function for parameters appropriate to the V994 Her system. The abscissa and the ordinate are the initial values of $\mathcal{J}_{\rm A}$ and $\mathcal{J}_{\rm B}$ inclinations of the orbital planes of systems A and B with respect to the orbital plane of their mutual motion. See the text for more discussion.

Fig. 1 shows the results. For sake of definiteness, we used nominal parameters of the V994 Her system (Zasche & Uhlař 2016): (i) stellar masses $m_{\rm Aa} = 3.01\ {\rm M}_\odot$, $m_{\rm Ab} = 2.58\ {\rm M}_\odot$, $m_{\rm Ba} = 1.84\ {\rm M}_\odot$, $m_{\rm Bb} = 1.93\ {\rm M}_\odot$, and (ii) orbital periods $P_{\rm A} = 2.083\,27^{\rm d}$, $P_{\rm B} = 1.420\,04^{\rm d}$, and $P = 1062.8775^{\rm d}$. The eccentricities $e_{\rm A}$ and $e_{\rm B}$ of the A and B systems were assumed zero, and the eccentricity of their mutual motion $e = 0.76$. When $\mathcal{J}_{\rm A} \simeq \mathcal{J}_{\rm B}$ we have $F > 0$ up to values of 0.6–0.8. This translates into maximum angular separation of the A and B planes being only 20–40 per cent of the plain sum $(\mathcal{J}_{\rm A} + \mathcal{J}_{\rm B})$, making them to be significantly more coupled together.

Fig. 2 shows an example of numerical integration that illustrates our conclusion. We keep using physical and orbital parameters of the V994 Her system determined by (Zasche & Uhlař 2016). In particular, the inclinations of the two eclipsing binaries were estimated to be $i_{\rm A} \simeq 84^\circ$ and $i_{\rm B} \simeq 85^\circ$. Zasche & Uhlař (2016) also argued that the inclination of their relative orbit must be large, but were not able to determine its value precisely; for simplicity, we assume $i \simeq 90^\circ$. Obviously, this is only half of the information needed to set the mutual architecture of the three orbital planes, as we need to specify nodal longitudes. Unfortunately, the available photometric and spectral observations cannot determine these parameters, and the exact mutual inclinations of the three planes are not presently known. In what follows we test different assumptions. Motivated by our discussion above, we start with a small value of mutual inclinations. Therefore, assigning arbitrarily $\Omega = 0^\circ$ (note the origin of Ω is irrelevant for the mutual inclination of the orbital planes), we next assume $\Omega_{\rm A} = 10^\circ$ and $\Omega_{\rm B} = 15^\circ$. This results in $\mathcal{J}_{\rm A} \simeq 11\overset{\circ}{.}6$ and $\mathcal{J}_{\rm B} \simeq 15\overset{\circ}{.}8$ initially. For these values we have $\mathcal{J}_{\rm AB}^{\rm max} \simeq 5\overset{\circ}{.}2$, or $F \simeq 0.8$ (see also Fig. 1). To make the comparison of the results as close as possible, we now assume zero eccentricities $e_{\rm A}$ and $e_{\rm B}$, and

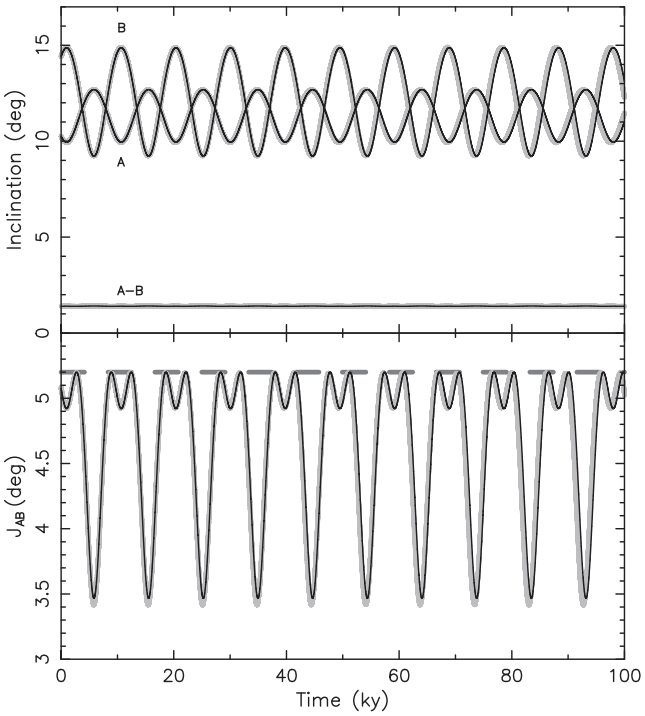

Figure 2. Exemplary numerical integration of a V994 Her-like system with the A and B orbital planes tightly coupled. Grey line from a complete numerical integration of the Hamiltonian (1), black line from numerical integration of the secular system (12)–(17). Top: orbital inclination with respect to the Laplace plane (normal to the conserved total angular momentum) for A and B systems (labels A and B), and the mutual motion of B about A (label A-B). Bottom: mutual inclination $\mathcal{J}_{\rm AB}$ of the A and B orbital planes; the dashed grey line at $\simeq 5\overset{\circ}{.}2$ is the analytically derived limit $\mathcal{J}_{\rm AB}^{\rm max}$.

keep the large value for the eccentricity $e = 0.76$ of the systems A and B relative orbit. The corresponding argument of pericentre is $\omega \simeq 236^\circ$ from Zasche & Uhlař (2016).

We used two integrators for interest of their comparison: (i) direct integration of Hamilton's equations derived from Hamiltonian (1), and (ii) integration of secular system (12)–(17). The secular system obviously contained only the quadrupole and octupole interaction terms (18) and (21), but it runs approximately two orders of magnitude faster. The match of the results from both numerical models is very good. All orbital variables were transformed into the Laplace coordinate system with (i) the z-axis along the direction of the conserved total angular momentum of the system, and (ii) the x-axis along the nodal line of the A and B systems (the nodal line of their mutual motion is then directed along $-x$). First we confirm that $e_{\rm A}$ and $e_{\rm B}$ remain essentially zero except for a very low-amplitude oscillations. Similarly, the eccentricity e of the mutual motion of A and B centre-of-mass is conserved. The inclination values of the A and B orbital planes with respect to the Laplace plane xy show long-period oscillations (Fig. 2, top panel). However, their nodal circulation in this reference frame is coupled enough such that the mutual inclination $\mathcal{J}_{\rm AB}$ of A and B orbital planes oscillates between $\simeq 3\overset{\circ}{.}5$ and $\simeq 5\overset{\circ}{.}2$ (Fig. 2, bottom panel). The analytical limit $\mathcal{J}_{\rm AB}^{\rm max}$ is shown by the grey dashed line at the bottom panel of Fig. 2, and indeed it nicely bounds the oscillations of $\mathcal{J}_{\rm AB}$ angle.

One may wonder, whether the time-scale shown in Fig. 2 is sufficient for our conclusion of a persisting coplanarity of the A and B orbital planes. This is because equations (26) and (27) basically indicate that $\boldsymbol{k}_{\rm A}$ and $\boldsymbol{k}_{\rm B}$ precess about a near constant $\boldsymbol{k}$ with frequencies $\sigma_1 \cos \mathcal{J}_{\rm A}$ and $\sigma_2 \cos \mathcal{J}_{\rm B}$. By coincidence their ratio is near unity to about a per cent level. As a result one could think that non-coplanarity would develop on a time-scale of $\simeq$(100–1000) precession cycles of the A and B planes in the Laplace frame. We thus repeated our simulation to 100 Myr, instead of 100 kyr shown on Fig. 2. It turns out that the system keeps to be very stable even on this much longer time-scale and no long-term oscillations in $\mathcal{J}_{\rm AB}$ angle are observed.

3 NUMERICAL EXAMPLE: V994 HER

3.1 The point-mass model

We now extend the previous analysis by (i) dropping the restriction of zero eccentricities of the A and B orbits, and (ii) exploring dependence of the results on changes in geometrical architecture of the system (mutual inclinations of the three orbits). As we continue using V994 Her to be our template for the 2+2 multiple stellar system, we now adopt the observed values of the eccentricities of the eclipsing binaries (Zasche & Uhlař 2016): $e_{\rm A} \simeq 0.031$ and $e_{\rm B} \simeq 0.125$. Variations of the orbital architecture are easily achieved by changing nodal longitudes $\Omega_{\rm A}$ and $\Omega_{\rm B}$.

To proceed step-by-step, and to not confuse different effects together, we first relax the eccentricity values of the eclipsing systems $e_{\rm A}$ and $e_{\rm B}$ mentioned above. We also use the corresponding arguments of pericentre $\omega_{\rm A} \simeq 10^\circ$ and $\omega_{\rm B} \simeq 301^\circ$ from Zasche & Uhlař (2016), all of the MJD 53855 epoch. Fig. 3 shows the results. Recall the inclinations in this figure have been transformed to the Laplace frame, in which the z-axis is directed along the conserved total angular momentum of the system. Upper and lower panels are as in Fig. 2, while the middle panel now shows evolution of the orbital eccentricities of the A and B binaries (the eccentricity $e = 0.76$ of their mutual orbit is conserved). As above, the grey lines are from full-fledged numerical integration of the system (including the short-period orbital effects), and the black line results from a much faster integration of the secular system (12)–(17) with quadrupole and octupole perturbations included. Clearly, this orbital architecture is fairly stable, with $e_{\rm A}$ and $e_{\rm B}$ values having just small-amplitude oscillations. This is because the mutual angles $\mathcal{J}_{\rm A}$ and $\mathcal{J}_{\rm B}$ of the A and B orbits with respect to the A-B plane are smaller than $\sim 15^\circ$. The mutual angle $\mathcal{J}_{\rm AB}$ of the A and B orbital planes exhibits stable oscillations between $\simeq 1^\circ$ and $\simeq 6^\circ$, still being fairly well bounded by the simple analytic estimate $\mathcal{J}_{\rm AB}^{\rm max}$ (dashed grey line at the bottom panel). This is because ≤ 0.15 eccentricities of the A and B orbits only little affect the overall dynamics of the system.

As expected, things change when the inclinations of A and B in the Laplace frame approach $\simeq 40^\circ$, namely the Kozai instability limit. To probe onset of this regime, we chose $\Omega_{\rm A} = 35^\circ$ and $\Omega_{\rm B} = 40^\circ$ in our next simulation. Other orbital elements at the initial epoch were as above. Results of the orbital propagation for these initial data are shown in Fig. 4. Now the initial values of the relative inclinations $\mathcal{J}_{\rm A}$ and $\mathcal{J}_{\rm B}$ are $\simeq 35^\circ$ and $\simeq 40^\circ$, the latter being larger than the critical Kozai inclination (e.g. Farago & Laskar 2010). In the point-mass model at this stage the eccentricities $e_{\rm A}$ and $e_{\rm B}$ behave differently: while $e_{\rm A}$ is still stable, $e_{\rm B}$ exhibits large oscillations that also trigger similar inclination effects. The orbital planes of the A and B orbits now decouple and their mutual angle $\mathcal{J}_{\rm AB}$ spans a large interval of values from 0° to more than $\simeq 70^\circ$. Obviously, at this moment the analytical limit $\mathcal{J}_{\rm AB}^{\rm max}$ is of no use, because the basic simplifying assumptions in Section 2.3 are violated.

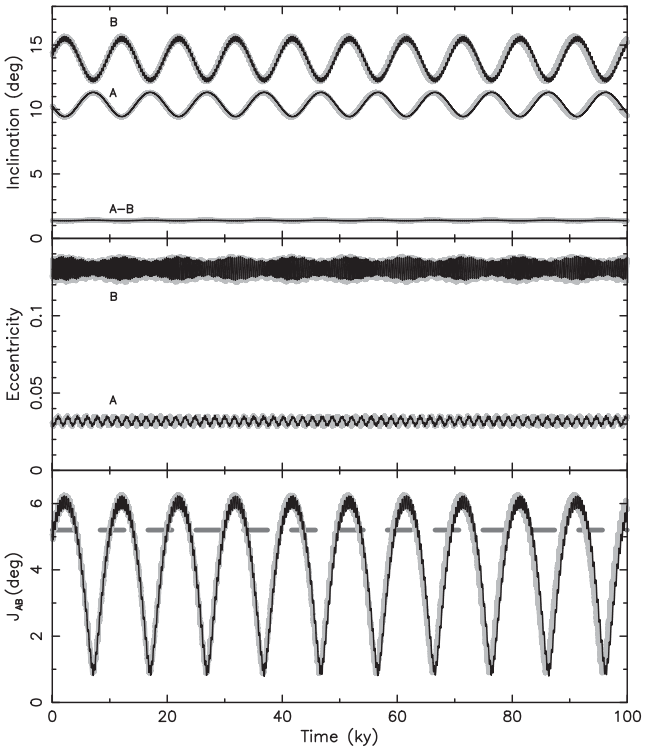

Figure 3. Exemplary numerical integration of a V994 Her-like system with the A and B orbital planes tightly coupled. Grey line from a complete numerical integration of the Hamiltonian (1), black line from numerical integration of the secular system (12)–(17). Contrary to Fig. 2, here we initially adopt true eccentricities of the eclipsing systems $e_A \simeq 0.031$ and $e_B \simeq 0.125$. Top: orbital inclination with respect to the Laplace plane (normal to the conserved total angular momentum) for A and B systems (labels A and B), and the mutual motion of B about A (label A-B). Middle: orbital eccentricities of the A and B systems. Bottom: mutual inclination $\mathcal{J}_{AB}$ of the A and B orbital planes; the dark grey line at $\simeq 5\overset{\circ}{.}2$ is the formal, analytically derived limit $\mathcal{J}_{AB}^{max}$.

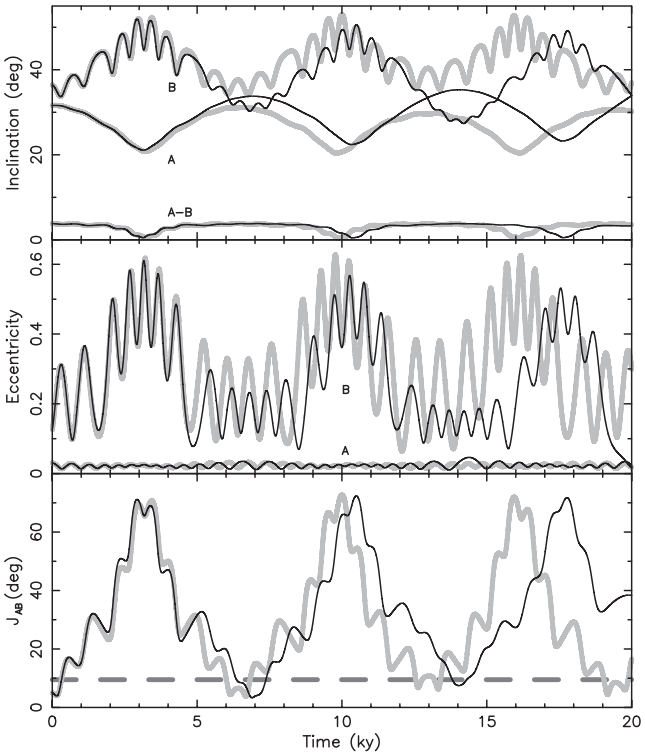

Figure 4. The same as in Fig. 3, but now in the situation when the orbital inclinations are large. This is particularly important for the system B. Top panel shows inclination values in the Laplace frame, in which i_B exceeds 40°, a limit for onset of Kozai-type dynamics. In this regime, inclination and eccentricity undergo large-amplitude, correlated oscillations. This is demonstrated in the middle panel, where e_B maximum values reach above 0.6. The mutual inclination $\mathcal{J}_{AB}$ of the A and B orbital planes (bottom panel) now attains large values, exceeding the simple limit $\mathcal{J}_{AB}^{max}$ from the zero-eccentricity analysis in Section 2.3. While initially results of the full numerical integration and the secular approximation agree well, they start to significantly deviate after $\simeq$5 kyr.

Fig. 4 also indicates that, unlike in the previous cases, results from the direct numerical integration of the Hamilton's equations and the secular system no more agree beyond ∼5 kyr. Fig. 5 helps to further grasp the situation: here we show time dependence of the argument of pericentre ω for the three orbits A, B and A-B in the observer-oriented frame (i.e. measured from the sky plane as it is traditional in stellar astronomy). The phase space describing orbital motion of the quadruple system has now quite more complex structure. Previously, these elements were only slowly, but steadily circulating. This is now continued on the time-scale shown in the figure only by the argument of pericentre of the mutual orbit of the two binary systems. The corresponding element of the A and B binaries has far more complex evolution. The periods of circulation are interrupted by oscillations and vice versa. This reflects existence of additional stable and unstable solutions in the phase space and the chaotic zones near the separatrix of their associated libration and circulation regions (Farago & Laskar 2010).

As a rule of thumb, that we also want to illustrate here, the best understanding of dynamical features is obtained if the elements are transformed to the Laplace frame (i.e. with the z-axis along the conserved total angular momentum of the whole system). Fig. 6 shows argument of pericentre for orbits A and B in this reference frame. While ω_A for the system A behaves nearly regularly, showing a near-steady circulation because its inclination in this frame is

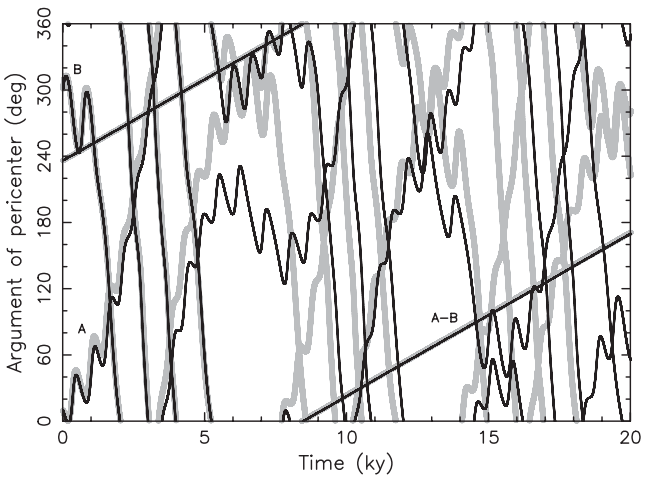

Figure 5. Time evolution of argument of pericentre ω for the three orbits, A and B (the close binaries) and A-B (mutual orbit of the binaries) in the observer-oriented frame. The steady circulation pattern now changes to irregular evolution with temporary reversals for the orbits A and B. Prediction from the full numerical model starts to deviate from that of the secular theory at ∼5 kyr.

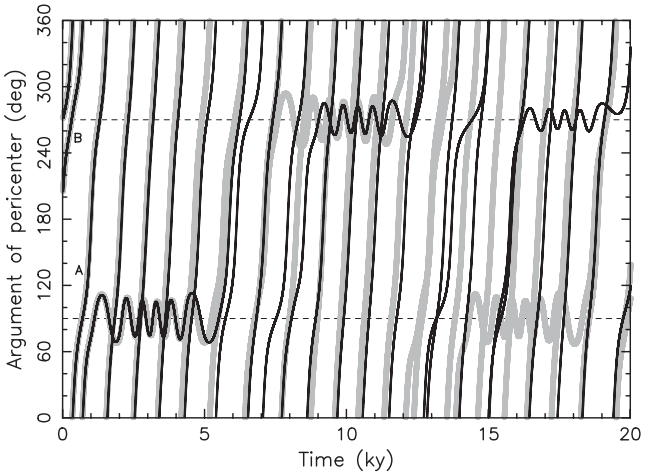

Figure 6. Time evolution of argument of pericentre ω for the two binary orbits of V994 Her system, A and B, in the Laplace frame. While $\omega_{\rm A}$ is characterized by a nearly steady circulation, $\omega_{\rm B}$ shows intermittently periods of circulation and librations, when captured around the stationary points at 90° and 270°. The grey lines from the complete numerical simulation, the black lines from integration of the secular system.

subcritical, $\omega_{\rm B}$ has a much more irregular evolution, related to its super-critical inclination. Circulation is soon interrupted by capture of librations about the stationary point at 90°. However, this capture is only temporary. At about 5 kyr in the integration it is left for another period of circulation, before being captured anew, now about the stationary point at 270°. These periods of captures about 90°/270° stationary points proceed with transition through a chaotic layer in the phase space. That is where the full numerical model and the simplified secular model start to diverge.

3.2 Beyond the point-mass model: order restored

Results described in our second example above (large relative inclination values $\mathcal{J}_{\rm A}$ and $\mathcal{J}_{\rm B}$), while theoretically interesting, suggest the point-mass model must be incomplete, provided the so far unknown mutual inclination of the orbits is large. Not only the apparent instability of the whole system would be striking, but also the peak eccentricities for the B system of ∼0.6 are not possible as they would imply stellar collision. Suffice, however, to notice that the pericentre precession period for both eclipsing binaries would become several thousand years long in the observer-oriented system (Fig. 5). This is in conflict with the observationally suggested precession periods of 116 ± 50 yr for the A system and 111 ± 40 yr for the B system. We note that even in the low $\mathcal{J}_{\rm A}$ and $\mathcal{J}_{\rm B}$ case discussed earlier in Section 3.1, the four-body interaction induces precession periods of pericentres of the A and B systems would be about 10 times longer than observed. So at least 90 per cent of this effect must come from somewhere else.

The proximity of the components in the eclipsing binaries offers a natural solution. While the point-mass model provides a basis of the orbital solution, dynamics of the A and B systems requires to include interaction terms of stars modelled as extended bodies, including their tidal integration. This task can be performed at different level of accuracy. Given the large parametric uncertainty in V994 Her we restrict to a simple quadrupole model by Hut (1981) at this moment.[6]

This implies that the dynamical equations of the A system, as they follow from the Hamiltonian (1), are complemented by a term

$$\left(\frac{{\rm d}\boldsymbol{p}_{\rm A}}{{\rm d}t}\right)_{\rm quadr} = -\frac{6\,Q_{\rm A}}{1-Q_{\rm A}}\,G\,\frac{m'_{\rm A}M_{\rm A}}{r_{\rm A}^3}\left(\frac{\mathcal{R}_{\rm A}}{r_{\rm A}}\right)^5\boldsymbol{r}_{\rm A}, \tag{37}$$

where $\mathcal{R}_{\rm A}$ is a characteristic radius and $Q_{\rm A}$ is a characteristic quadrupole deformability of stars in the A system. One could also split (37) into two terms representing tide produced by Ab on Aa components, and vice versa, but again such details are not essential at this time. Such contribution translates into a corresponding term, by which the secular system has to be complemented. A simple algebra yields (e.g. Eggleton, Kiseleva & Hut 1998; Eggleton & Kiseleva 2001; Fabrycky & Tremaine 2007; Liu et al. 2015)

$$\left(\frac{{\rm d}\boldsymbol{\pi}_{\rm A}}{{\rm d}t}\right)_{\rm quadr} = F_{\rm A}\,(\boldsymbol{K}_{\rm A}\times\boldsymbol{\pi}_{\rm A}), \tag{38}$$

with

$$F_{\rm A} = n_{\rm A}\frac{15\,Q_{\rm A}}{1-Q_{\rm A}}\left(\frac{\mathcal{R}_{\rm A}}{a_{\rm A}}\right)^5\frac{1+\frac{3}{2}e_{\rm A}^2+\frac{1}{8}e_{\rm A}^4}{\eta_{\rm A}^{11}}, \tag{39}$$

A similar terms should also complement description of dynamics of the B system.

For sake of our test, we assumed mass–radius relation $\mathcal{R}\propto M^{0.8}$ for stars in the A and B binaries. The quadrupole deformability values $Q_{\rm A}\simeq0.031$ and $Q_{\rm B}\simeq0.014$ were set to match the above-mentioned precession rates in the binary components of the V994 Her system. Assuming the same initial conditions as used in simulation shown in Fig. 4, but now including the quadrupole interaction from (38), we obtain orbital evolution shown in Fig. 7. As anticipated, order has been restored with now only small oscillations in the orbital inclinations of orbital planes of the A and B binaries (top panel). Their mutual angle $\mathcal{J}_{\rm AB}$ (bottom panel) also indicates only limited variations. Interestingly, the upper limit $\mathcal{J}_{\rm AB}^{\rm max}$ derived in Section 2.3 for point-mass model still holds well (grey line in the bottom panel). This is because the quadrupole model is basically still valid for the orbital planes dynamics, thus $\boldsymbol{k}$, $\boldsymbol{k}_{\rm A}$, and $\boldsymbol{k}_{\rm B}$ vectors. Their dynamics is not affected by the star–star quadrupole interaction in the close binaries A and B as seen from equation (38). This effect principally enforces fast pericentre circulation in the binaries, inhibiting thus the long-term Kozai instability seen in Fig. 4. There is again good agreement between prediction of the orbit evolution by the full numerical model and the secular system.

To further illustrate persistent near-coplanarity of the orbital planes of the binaries A and B we show in Fig. 8 orbital inclinations $i_{\rm A}$ and $i_{\rm B}$ in the observer-oriented system (i.e. measured with respect to the sky-plane). Because their orbital inclinations with respect the orbital plane of their relative motion, that has $i=90°$, are ≃(30°–40°) (Fig. 7), the inclinations in the observer-oriented frame oscillated between ≃(60° and 120°). This is a simple projection of the orbital precession in the Laplace system. Interestingly though, the oscillations have nearly the same frequency such that both A and B systems are either eclipsing or, occasionally, non-eclipsing. In ≥95 per cent of time this happens simultaneously.

In conclusion, we note that until interferometric observations reveal more details about the orbit-plane architecture of the V994 Her system, all possibilities are in principle open (i.e. from coplanar to perpendicular orbit planes of A and B with respect to each other and

[6] Note, however, that the essential fast component in the precession of orbital pericentres for the A and B system in rather independent on specific details of the model. we also do not include the tidal component in the Hut's model, since it is not necessary for the sake of our argument.

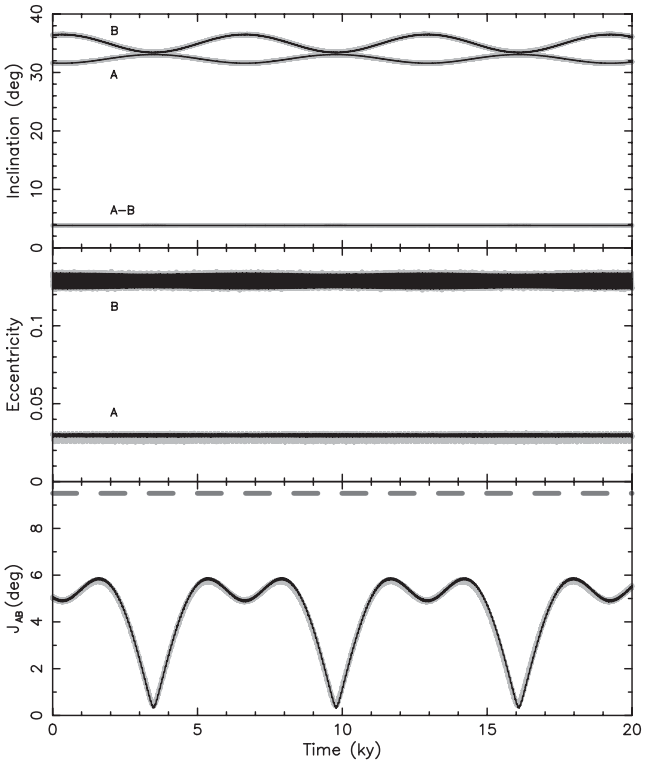

Figure 7. The same as in Fig. 4, but now the model contains apart from the mutual gravitational interactions of the stars as mass points also quadrupole interactions between the components in the close binaries A and B (see equation 38). The quadrupole deformability parameters Q_A and Q_B were adjusted such that the pericentres of the binary systems circulate with the observationally constrained periods. This restores the order with only small oscillations of the inclinations and eccentricities. The orbital planes of the binaries remain close each other (bottom panel); the dashed grey line is the formal limit $\mathcal{J}_{AB}^{max}$ from the zero-eccentricity analysis in Section 2.3.

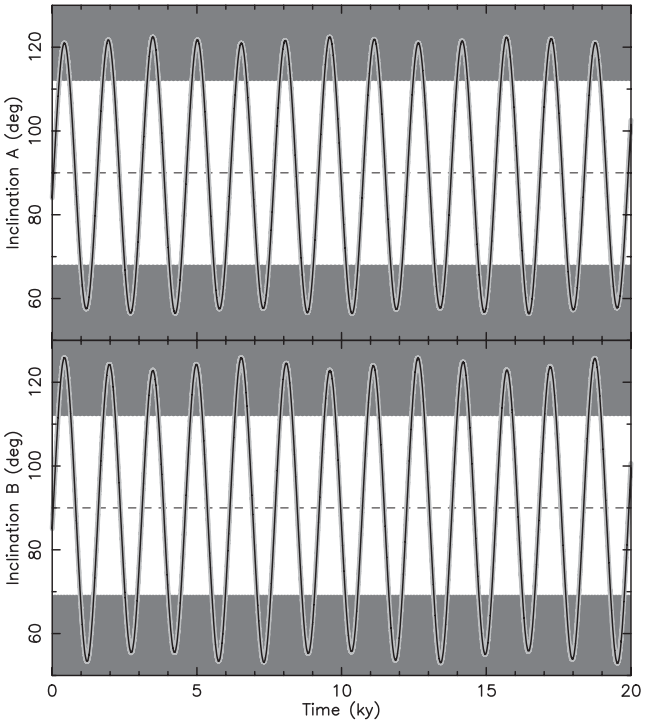

Figure 8. Inclination of the orbital plane for binaries A (top) and B (bottom) in the observer-oriented coordinate system (dynamical model from Fig. 7). The bold grey line is from complete numerical integration, the black line is from numerical integration of the secular system. The dark grey region indicates inclination for which no eclipses in the binaries would be observed.

with respect to the plane of A-B motion). However, and interesting clue could be provided by a rather high eccentricity of the B system: $e_B \simeq 0.125$ (Zasche & Uhlař 2016). We speculate it could have to do with the mutual interaction of the A and B components in the system. This would favour non-coplanar configuration. Analysis of systems predicting the observed e_B value, obviously in a statistical sense, could provide interesting constraints on the tidal interaction of the stars in the B system.

3.3 Statistics of eclipses in the V994 Her-like systems

Encouraged by a rather good performance of the secular numerical model, and intrigued by previously described tight coplanarity of the A and B orbital planes in our previous simulations, we now proceed to show usefulness of the secular model in dealing with more general problems. We should recall that its principal strength is in the possibility to choose a much longer integration timestep than in the fully numerical model, allowing a much faster performance.

The problem we want to analyse is a general statistical expectation of occurrence of eclipses in the V994 Her-like quadruple systems in 2 + 2 hierarchy. For simplicity we shall assume parameters from our simulation shown in Fig. 7, obviously except for the orbital plane inclinations and node longitudes. In particular, we keep the mean orbital periods P_A, P_B, and P from above, as well as the stellar masses m_{Aa}, m_{Ab}, m_{Ba}, and m_{Bb}. The latter also set the assumed stellar radii of approximately $\mathcal{R}_{Aa} \simeq 2.4\ R_\odot$, $\mathcal{R}_{Ab} \simeq 2.1\ R_\odot$, $\mathcal{R}_{Ba} \simeq 1.6\ R_\odot$, and $\mathcal{R}_{Bb} \simeq 1.7\ R_\odot$. For sake of definiteness, we also keep the eccentricity values e_A, e_B, and e, and the quadrupole deformabilities Q_A and Q_B. Obviously, the simulation can be efficiently performed with different values of these parameters, but here we limit ourselves to a demonstration of the method rather than a complete scan of results through a large parameter space.

First, we consider a static situation. This will provide a useful template for comparison when discussing results of the more general dynamical model. Assuming thus no mutual interactions between the A and B systems, as if they were isolated, we can simply evaluate odds for each of them separately to be eclipsing. This is only set by orbital periods, eccentricities, and stellar radii (assuming their spherical shape). Assuming the orbital planes are isotropic in space, we find there is $\simeq$36.6 per cent chance that system A is eclipsing and $\simeq$39.7 per cent chance that the system B is eclipsing. Considering these two probabilities uncorrelated, there is $\simeq$14.5 per cent chance that both systems A and B are simultaneously eclipsing. Obviously, in this simplified model the systems are either eclipsing or not, and keep being so independently of time.

Moving to real life, we have to take into account that the systems A and B inevitably interact. Examples of their orbital evolution have been shown in the previous section. Therefore, we now run a simulation with all orbital components evolving as predicted by the secular model. For sake of simplicity, the initial orbital planes of A, B, and A-B components were set isotropic in space.[7] We ran 10^5 trial

[7] Note that the early evolution of the quadruple systems during their initial contraction may result in a more complex than isotropic distribution of the orbital planes. Analysis of this effect is beyond the scope of this paper.

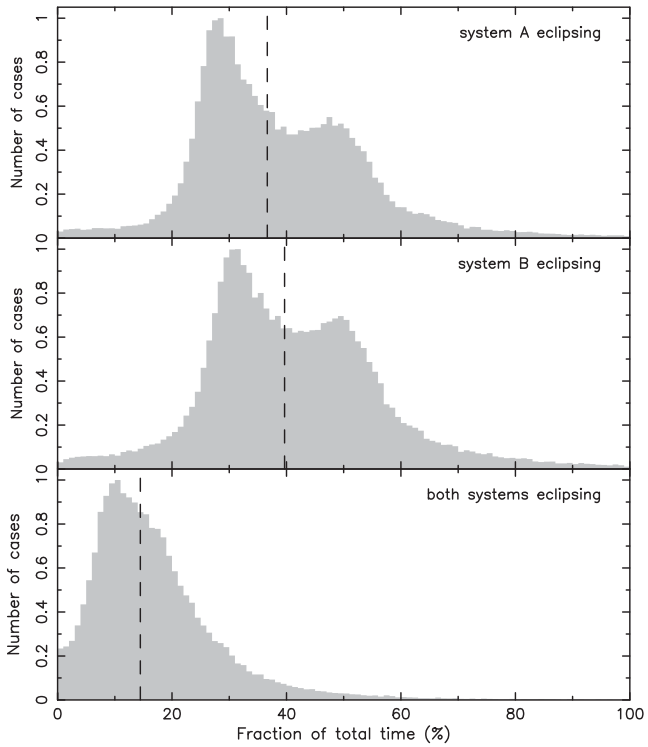

Figure 9. Results from a 50 kyr integration of 10^5 trial evolutions of V994 Her-like systems with initially isotropic distribution of orbit planes for all components (A, B and A-B) in space. The grey histogram at each of the panels shows statistical distribution of what fraction of the total time a particular component was eclipsing: (i) system A at the top, (ii) system B in the middle, and (iii) both systems A and B simultaneously at the bottom (distributions were arbitrarily normalized to unity). The dashed lines show what is the expected occurrence in a static model, in which the orbits would not evolve in time: 36.6 per cent for the system A, 39.7 per cent for the system B, and 14.5 per cent for both systems simultaneously. The median values of each of the distributions are very close to these values.

simulations, each lasting 50 kyr, with a timestep of 10 d (in fact conservatively short). At each timestep we monitor the configuration of the orbital planes for all three components in the system and determine whether systems A and B are eclipsing at that epoch. Because the system dynamically evolves, the eclipses in a given individual trial run may persist, occur transiently or never, depending on the direction to the observer. Note, however, that our overall results obviously do not depend on the observer's position because of isotropy of the initial conditions of our simulation. Having recorded at each epoch, and for each trial run, existence or inexistence of eclipses, we can finally determine statistical distribution of their appearance for the A and B systems, or both together.

Fig. 9 shows our results. First, we note that the system A had eclipses in at least one instant during our individual trial simulations in $\simeq$91.8 per cent cases, the system B in $\simeq$93.7 per cent cases, and both systems together in $\simeq$83.9 per cent cases. Conversely, the system A had never eclipses during the monitored 50 kyr interval of time in $\simeq$8.2 per cent cases, the system B in $\simeq$6.3 per cent cases, and simultaneous eclipses of systems A and B never happened in $\simeq$16.1 per cent cases. The trial runs in which some eclipses occurred were used to construct distributions shown in the Fig. 8. In particular, for each of the simulations we evaluated percentage of the total time in which the particular component was eclipsing. Interestingly, the median values of these distributions are within uncertainty the same as those determined for the static model (see above). The distributions are, however, quite broad and have tails towards large and small values. We are mainly interested in the cases that showed abundance of eclipses of both systems A and B. Checking some of the trial runs that resulted in this behaviour, we observed they indeed correspond to the near coplanar configurations described in Sections 3.1 and 3.2, for which the observer happened to be close to the orbital plane of the relative A-B motion. In quantitative terms, there is $\simeq$1.7 per cent chance that both systems A and B are simultaneously eclipsing for more than 50 per cent of time.

4 KOZAI–LIDOV REGIME FOR THE QUADRUPLES: AN EXEMPLARY CASE

Another example of a useful application of our secular model for the 2+2 quadruple systems is a more in-depth analysis of the KL regime, whose some aspects were already mentioned in Section 3.1. The many applications of the KL dynamics have attracted a lot of attention over the past decade or so. Their original area bound to the Solar system dynamics has largely opened to many other fields in astronomy, including important results in exoplanet dynamics and astrodynamics. Naoz (2016) provides a recent and fairly complete review of many of them. While we do not intend to enter the vast realm of KL dynamics applications in this paper, we briefly show that our formulation is fully capable to recover some of the earlier-published results with a significant CPU time gain characteristic to the secular versus complete integration.

One of the interesting aspects of the KL dynamics is a possibility to flip orientation of the participating orbits from prograde to retrograde sense and vice versa (e.g. Naoz 2016, and references therein). In the simpler case of triples, this phenomenon does not occur in the first-order secular theory when only the quadrupole interaction term is included. One needs a contribution from the octupole interaction term to provide the necessary degree of freedom in the solution (e.g. Katz, Dong & Malhotra 2011; Luo, Katz & Dong 2016; Naoz 2016). However, when all masses of the participating objects are equal the secular effect of the octupole terms disappears and the desired flips are again banned. The situation is more complex for quadruple systems. Staying with the 2 + 2 hierarchy, one could investigate the interplay of the A and B systems and analyse their orientation with respect to the relative orbit A-B. In Section 2, we have demonstrated that this could be to a high degree of accuracy modelled as two interacting triple systems. Therefore, even when considering all masses equal, for which the octupole terms are nil, the phenomenon of orbit A or B flipping may occur at the expense of interaction of the systems. This effect has been pointed out by Pejcha et al. (2013), who used a complete numerical model in their study. Here we show that their results are easily recovered also using our secular model with, obviously, a significant gain in computation time.

We first tested capability of our secular scheme by choosing the initial orbital data similar to those in bottom panel of fig. 1 of Pejcha et al. (2013), except for the secular angles, which were not reported in this reference. Specifically, we set all stellar masses equal to the solar mass ($m_{\rm Aa} = m_{\rm Ab} = m_{\rm Ba} = m_{\rm Bb} = 1$ M$_\odot$), and used $a_{\rm A} = 0.57$ au, $a_{\rm B} = 0.35$ au, and $a_{\rm AB} = 5$ au for the corresponding semimajor axes. Initial eccentricity values were $e_{\rm A} = 0.3$, $e_{\rm B} = 0.1$, and $e_{\rm AB} = 0.3$. Additionally, in accord with Pejcha et al. (2013), we had initially $\cos \mathcal{J}_{\rm A} = 0.3$ and $\cos \mathcal{J}_{\rm B} = -0.05$, where $\mathcal{J}_{\rm A}$ and $\mathcal{J}_{\rm B}$ are relative inclinations of the A and B orbital planes with respect to the orbital plane of A-B orbit. Other orbit parameters, longitude

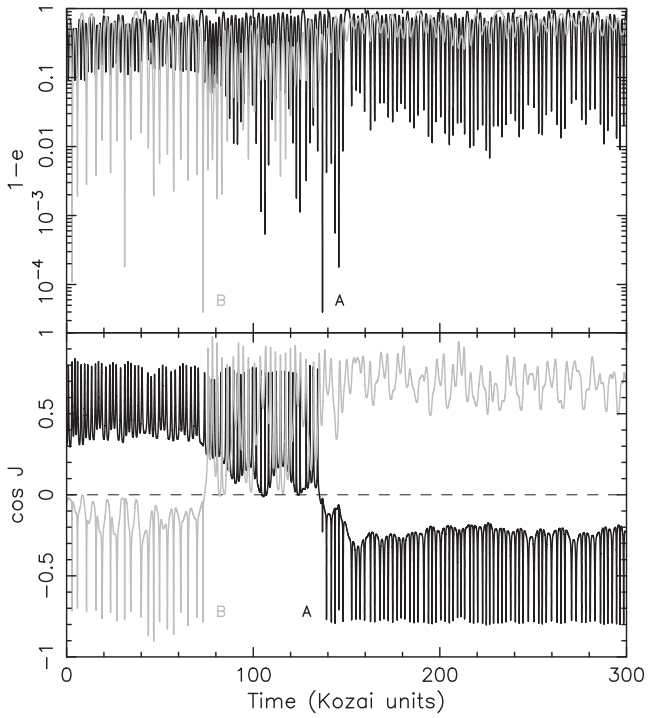

Figure 10. Illustration of a chaotic behaviour of eccentricities (top) and relative inclinations (bottom) of the A and B systems with respect to the A-B orbital plane in a deep Kozai regime. Solution for the A system is shown in black, solution for the B system in grey colour. Time at the abscissa is given in the Kozai unit $t_{\rm K}$, here about 37.8 yr. Quadruple nature of the system allows orbital flips even for equal-mass case assumed in this simulation ($m_{\rm Aa} = m_{\rm Ab} = m_{\rm Ba} = m_{\rm Bb} = 1\,{\rm M}_\odot$). Other orbital parameters as in fig. 1 (bottom panel) of Pejcha et al. (2013).

of node and pericentre for all orbits were chosen randomly. We numerically integrated equations of the secular system for about 11 kyr with a timestep of 0.1 yr. In accord with Pejcha et al. (2013), we scaled time in our solution by the Kozai unit $t_{\rm K}$:

$$t_{\rm K} = \frac{2}{3\pi}\left[\frac{a_{\rm A}\left(1-e_{\rm AB}^2\right)}{a_{\rm B}}\right]^{3/2}\left[\frac{a_{\rm AB}}{a_{\rm A}}\right]^3 P_{\rm B}. \qquad (40)$$

In our case, $t_{\rm K} \simeq 37.8$ yr, thus our solution had approximately $300\,t_{\rm K}$. Fig. 10 shows eccentricities $e_{\rm A}$ and $e_{\rm B}$, together with relative inclinations $\mathcal{J}_{\rm A}$ and $\mathcal{J}_{\rm B}$ as a function of time, and could be thus directly compared with fig. 1 of Pejcha et al. (2013). Obviously, details are not the same, since the initial secular angles of our solution were most likely different. Additionally, the chaotic evolution near the flip conditions would anyway produce difference between the fully numerical results of Pejcha et al. (2013) and our solution. These details are, however, not important here. What matters more is the general character of the solution, namely large oscillations of the eccentricities and orbit flips when one of them approaches unity. These qualitative features of the solutions are the same. We should mention that simulation in Fig. 10 took only a few seconds on a standard CPU core.

This is encouraging. To further illustrate usefulness of our approach we now re-derive the population results, namely spanning all possible initial values $\mathcal{J}_{\rm A}$ and $\mathcal{J}_{\rm B}$. In particular, we ran our propagator with $\cos\mathcal{J}_{\rm A}$ and $\cos\mathcal{J}_{\rm B}$ uniformly spanning 50 values in their definition intervals $(-1, 1)$. At each of these grid points we run 50 different jobs with secular angles chosen randomly. This is very similar to the procedure described by Pejcha et al. (2013), except for a more densely sampled $\cos\mathcal{J}_{\rm A}$ and $\cos\mathcal{J}_{\rm B}$ values in our simulation (which we can afford by faster speed of the runs). At each job we monitored behaviour of the eccentricities $e_{\rm A}$ and $e_{\rm B}$, in particular recorded cases when $1 - e_{\rm A}$ or $1 - e_{\rm B}$ became smaller than 10^{-3}. We found this happened in 31.0 per cent runs for the system A and 48.1 per cent runs for the system B. This is in a very good accord with 35.8 and 53.0 per cent cases reported by Pejcha et al. (2013) in their table 1. Fig. 11 shows $\cos\mathcal{J}_{\rm A}$ and $\cos\mathcal{J}_{\rm B}$ values for which system A (left) and system B (right) achieved these very high eccentricity states. The results are again in a very good accord with those shown by Pejcha et al. (2013) in their fig. 2.

While not exactly identical, our results therefore provide the same conclusions in a statistical sense as in Pejcha et al. (2013). However, there is a significant difference in the required CPU time: our simulation ran about 100 times faster.

5 CONCLUSIONS

Secular theory represents a versatile tool to study long-term evolution of stellar systems in different configurations. The most often discussed case is that of triple systems in the $2 + 1$ hierarchy. Here we extended this basic formulation to quadruple systems in the $2 + 2$ hierarchy.

Unless the systems are very compact, we found they could be effectively modelled as two interacting triple systems. This conveniently allows us to bring formulation of the secular equations of motion from triples, and easily adapt it to the more general case of quadruples. Our formulation may help to efficiently analyse data about the exceptionally tight and/or exceptionally well observed 2+2 systems, such as V994 Her or VW LMi (e.g. Pribulla et al. 2008; Pawlak et al. 2013). For instance, we estimate that the pericentre of the non-eclipsing component B in VW LMi may drift by $\simeq 3^\circ\,{\rm yr}^{-1}$ due to interaction with the system A. This is in a rough accord with the preliminary results reported by Pribulla et al. (2008), but more observations are clearly needed. Note that the $\simeq$7.93 d period of system B, and solar-mass stars, implies that the tidal or quadrupole interaction here would be quite less important than in the case of V994 Her system with shorter $P_{\rm A}$ and $P_{\rm B}$ values. The pericentre drift would be thus likely dominated by the four-body interaction described in our approach. Even more widely separated is the case of V379 Cep quadruple, where the systems A and B have orbital periods of $\simeq$99.8 d and $\simeq$158.7 d (e.g. Harmanec et al. 2007). Especially the non-eclipsing system B is interesting for us, because of its large estimated eccentricity of $e_{\rm B} \simeq 0.5$. If the whole architecture of this quadruple is not too distant from a coplanar case, we estimate that the pericentre of the system B should drift by about a degree in $\simeq$6 yr. A high-quality spectroscopy should be able to reveal this effect in about a decade or two. Obviously, interferometric and further photometric observations would be also valuable to characterize geometry of this interesting system.

The secular approach may be also efficiently used to study long-term evolutionary tracks during the formation phase of the quadruple systems. This includes orbital collapse powered by the tidal interaction during the high-eccentricity states excited by the angular momentum exchange between all components of the $2 + 2$ system (KL phase). This interesting application, awaiting further analysis, would require to complement secular equations presented in this paper by tidal and spin-orbit coupling effects as in Fabrycky & Tremaine (2007), who studied early phases of dynamical evolution for triples.

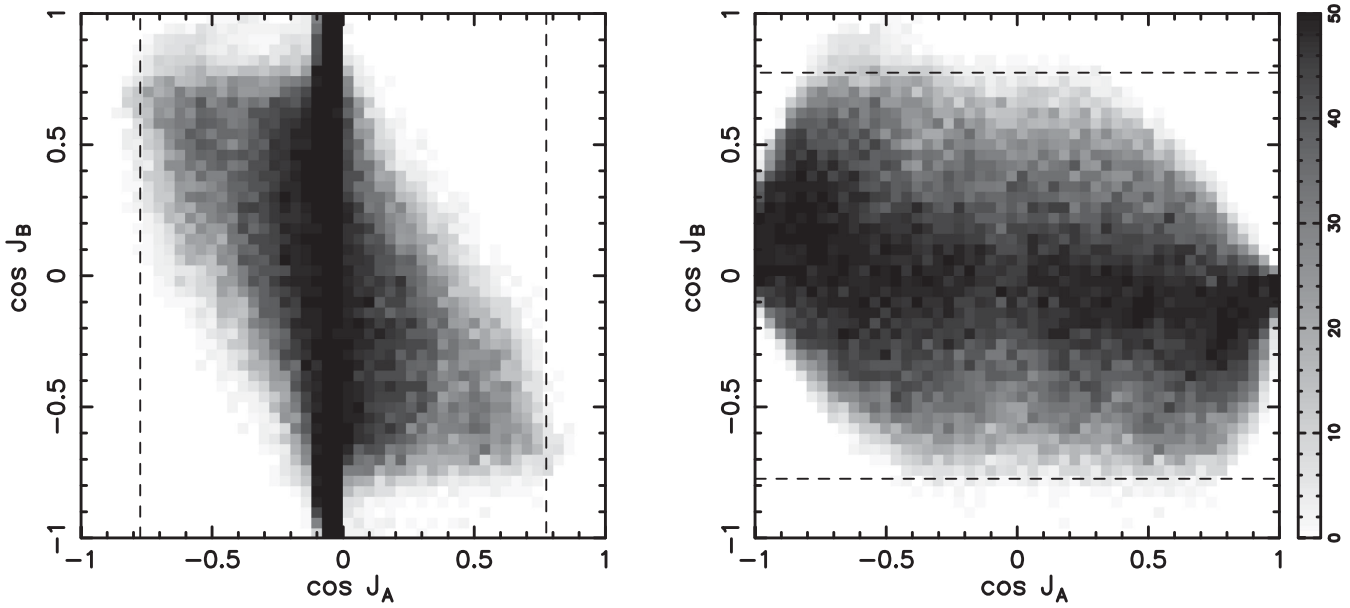

Figure 11. Simulations as in Fig. 10 now spanning a uniform grid of initial values cos $\mathcal{J}_A$ and cos $\mathcal{J}_B$ inclinations (abscissa and ordinate). The left-hand panel shows results for the system A, the right-hand panel for the system B. In both cases, we integrated 50 variants for each ($\mathcal{J}_A$, $\mathcal{J}_B$) grid-point, all having random values of secular angles (nodes and pericentres). In each job we monitored if $1 - e_A$ or $1 - e_B$ became smaller than 10^{-3}. Number of such cases are given by the grey-shaded plots with the value bar on the right of the figure. The dashed lines mark the formal Kozai angle cos $J_K = \pm\sqrt{3/5}$ for each system. The figure reproduces well results shown in fig. 2 of Pejcha et al. (2013).

ACKNOWLEDGEMENTS

I thank Petr Zasche for useful information about the V994 Her system and the anonymous referee for suggestions that helped to improve the final version of this paper. This work was partly funded through the research grants P209-13-01308S and GA15-02112S of the Czech Science Foundation.

REFERENCES

Beust H., 2003, A&A, 400, 1129
Breiter S., Ratajczak R., 2005, MNRAS, 364, 1222
Breiter S., Vokrouhlický D., 2015, MNRAS, 449, 1691
Cagaš P., Pejcha O., 2012, A&A, 544, L3
Eggleton P. P., Kiseleva-Eggleton L., 2001, ApJ, 562, 1012
Eggleton P. P., Kiseleva L. G. K., Hut P., 1998, ApJ, 499, 853
Fabrycky D., Tremaine S., 2007, ApJ, 669, 1298
Farago F., Laskar J., 2010, MNRAS, 401, 1189
Hamers A. S., Portegies Zwart S. F., 2016, MNRAS, 459, 2827
Harmanec P. et al., 2007, A&A, 463, 1061
Hut P., 1981, A&A, 99, 126
Katz B., Dong S., Malhotra R., 2011, Phys. Rev. Lett., 107, 18
Khodykin S. A., Zakharov A. I., Andersen W. L., 2004, ApJ, 615, 506
Kołaczkowski Z., Mennickent R. E., Rivinius T., Pietrzyński G., 2013, MNRAS, 429, 2852
Lee C.-U., Kim S.-L., Lee J. W., Kim C.-H., Jeon Y.-B., Kim H.-I., Yoon J.-N., Humphrey A., 2008, MNRAS, 389, 1630
Liu B., Muñoz D., Lai D., 2015, MNRAS, 447, 747
Luo L., Katz B., Dong S., 2016, MNRAS, 458, 3060
Milani A., Nobili A. M., 1983, Celest. Mech., 31, 241
Morbidelli A., 2002, Modern Celestial Mechanics. Taylor & Francis, London
Naoz S., 2016, Ann. Rev. Astron. Astrophys., preprint (arXiv:1601.07175)
Ofir A., 2008, Inf. Bull. Var. Stars, 5868, 1
Pawlak M. et al., 2013, Acta Astron., 63, 323
Pejcha O., Antognini J. M., Shappee B. J., Thompson T. A., 2013, MNRAS, 435, 943
Pribulla T., Baluďanský D., Dubovský P., Kudzej I., Parimucha Š., Siwak M., Vaňko M., 2008, MNRAS, 390, 798
Rosengren A. J., Scheeres D. J., 2014, Celest. Mech. Dyn. Astron., 118, 197
Roy A. E., Steves B. A., 2000, Celest. Mech. Dyn. Astron., 78, 299
Söderhjelm S., 1982, A&A, 107, 54
Széll A., Steves B., Érdi B., 2004, A&A, 427, 1145
Tokovinin A., 2008, MNRAS, 389, 925
Tokovinin A., 2014, AJ, 147, 87
Tremaine S., Touma J., Namouni F., 2009, AJ, 137, 3706
Zasche P., Uhlař R., 2013, MNRAS, 429, 3472
Zasche P., Uhlař R., 2016, A&A, 588, A121

This paper has been typeset from a TEX/LATEX file prepared by the author.